Two years online measurement of fine particulate nitrate in western Yangtze River Delta: Influences of thermodynamics and N_2O_5 hydrolysis

Peng Sun[1], Wei Nie[1,2,*], Xuguang Chi[1,2], Yuning Xie[1], Xin Huang[1,2], Zheng Xu[1,2], Ximeng Qi[1,2], , Zhengning Xu[1], Lei Wang[1], Tianyi Wang[1], Qi Zhang[3], and Aijun Ding[1,2,*]

[1]Joint International Research Laboratory of Atmospheric and Earth System Science s, and School of Atmospheric Sciences, Nanjing University, Nanjing, 210023, China
[2]Jiangsu Provincial Collaborative Innovation Center of Climate Change, Nanjing, 210023, China
[3]Department of Environmental Toxicology, University of California, Davis, CA 95616, USA
Correspondence: Wei Nie (niewei@nju.edu.cn) and Aijun Ding (dingaj@nju.edu.cn)

Abstract.

Particulate nitrate contributes a large fraction of secondary aerosols. Despite understanding of its important role in regional air quality and global climate, long-term continuous measurements are rather limited in China. In this study, we conducted online measurement of $PM_{2.5}$ nitrate for two years from March 2014 to February 2016 using the Monitor for Aerosols and Gases in ambient Air (MARGA) in the western Yangtze River Delta (YRD), eastern China, and investigate the main factors that influenced its temporal variations and formation pathways. Compared to other sites in China, an overall high concentration of particulate nitrate was observed with a mean value of 15.8 μg m^{-3} (0.5 to 92.6 μg m^{-3}). Nitrate on average accounted for 32% of the total mass of water-soluble ions and the proportion increased with PM loading, indicating that nitrate is a major driver of haze pollution episodes in this region. Sufficient ammonia drove most nitrate into the particle phase in the form of ammonium nitrate. A typical seasonal cycle of nitrate was observed with the concentrations in winter on average two times higher than those in summer mainly due to different meteorological conditions. In summer, the diurnal variation of particulate nitrate was determined by the thermodynamic equilibrium, resulting in a much lower concentration during daytime despite of a considerable photochemical production. Air masses from polluted YRD

and biomass burning region contributed to the high nitrate concentration during summer. In winter, particulate nitrate didn't reveal an evident diurnal variation. Regional transport from northern China played an important role in enhancing nitrate concentration. Eighteen nitrate episodes were selected to understand the processes that drive the formation of high concentration of nitrate. Rapid nitrate formation was observed during the pre-episode (the day before nitrate episode day) nights, and dominated the increase of total water-soluble ions. Calculated nitrate from N_2O_5 hydrolysis was highly correlated to and accounted for 80 percent of the observed nitrate, suggesting that N_2O_5 hydrolysis was a major contributor to the nitrate episodes. Our results suggested that rapid formation of nitrate could be a main cause for extreme aerosol pollution events in YRD during winter, and illustrated the urgent needs to control the NO_x emission.

1. Introduction

Particulate nitrate (NO_3^-), as a major aerosol component in the atmosphere, reduces atmospheric visibility (Charlson and Heintzenberg, 1995), influences human health, alters radiative forcing and hence influences regional even global climate (IPCC, 2013). Compared to the sulfate, nitrate has a larger scattering albedo under low RH conditions that cause a stronger influence on visibility (Lei and Wuebbles, 2013). High concentration of particulate nitrate had been demonstrated to be one of the major reasons for the frequent occurrence of haze episodes in China (Wang and Zhang, 2009; Wen et al., 2015; Wang et al., 2017). In recent decades, the Chinese government started to control emissions of air pollutants with special effort on the SO_2 reduction. This resulted in a remarkable decrease of ambient SO_2 and sulfate concentrations after 2006 (van der A et al., 2017; Wang et al., 2017). However, particulate nitrate, as well as its proportion in PM, showed increasing trends due to the strong emission of nitrogen oxides (NO_x) (Lei and Wuebbles, 2013; Yang et al., 2017).

Particulate nitrate can be formed from multiple pathways. Gas phase reaction of NO_2 and OH radical is one major pathway to form nitric acid (HNO_3) (Calvert and

Stockwell, 1983), which subsequently reacts with ammonia (NH_3) to produce ammonium nitrate (NH_4NO_3). As typical photochemical processes, these reactions dominate daytime nitrate formation, and have been widely investigated in both field and modelling studies (Sharma et al., 2007; Petetin et al., 2016). Heterogeneous uptake of the photochemical formed nitric acid by alkali compounds, e.g. dust and sea salt particles, is also a considerable pathway to form nitrate in some regions (Bian et al., 2014). During nighttime, the hydrolysis of dinitrogen pentoxide (N_2O_5) is believed to be the dominate pathway to form particulate nitrate. N_2O_5 is an important reactive nitrogen species in the polluted troposphere (Brown and Dube., 2007; Osthoff et al., 2006; Li et al., 2017; Brown et al., 2003; Brown and Stutz, 2012; Wang et al., 2016d; Wang et al., 2017b) and accumulates via the reversible reaction between NO_2 and NO_3 radical produced from the reaction of NO_2 with O_3. Due to the rapid photolysis of NO_3 radical, the contribution of N_2O_5 hydrolysis to nitrate concentration during daytime of sunny day is usually small. While during nighttime, N_2O_5 concentration can be up to ppb level, and form nitric acid by reaction with water vapor, or particulate nitrate directly by heterogeneous hydrolysis on the wet surface (Wang et al., 2017a; Wen et al., 2018; Thornton et al., 2003). In China, the pollution episodes with high nitrate concentrations mostly occurred in winter, during which the photochemical production of nitrate should be overall weak. N_2O_5 hydrolysis thus has the potential to be the crucial contributor, however there is still a lack of observational evidences.

Collecting particulate matter on a filter with subsequent ion chromatography analysis in laboratories is the conventional method to measure the concentration of particulate nitrate. The un-denuded filter pack system, which is most-widely used, can suffer from both positive artifacts by absorbing gas-phase nitric acid, and negative artifacts by the evaporation of ammonium nitrate (Nie et al., 2010; Pathak and Wu, 2009; Wang et al., 2010). A denuder system can minimize these sampling artifacts by adding denuders to remove the interfering gases and back-up filters to collect the evaporated vapers (John et al., 1988). However, the operation of such a denuder system

is extremely labor intensive and thus not widely used. In addition, the poor time-resolution of filter-based measurement can limit our understanding on the formation and chemical evolution of the particulate nitrate. To overcome these shortcomings, several continuous and semi-continuous techniques have been developed based on an online denuded-IC system (e.g. the ambient ion monitor (AIM), the gas and aerosol collector ion chromatography (GAC-IC), the particle-into-liquid sample ion chromatography (PILS-IC) and MARGA), as well as mass spectrometry (e.g. AMS). Pathak et al. (2011) applied an AIM instrument in Beijing and Shanghai for one month and found that the heterogeneous hydrolysis of N_2O_5 contributed 50%~100% of the nighttime nitrate formation. Xue et al. (2013) deployed a PILS-IC system in Hong Kong for less than a month and showed a more active nitrate formation during PM episode than normal days. Wen et al. (2015) used a MARGA instrument in Yucheng, North China during summer and emphasized the important roles of O_3 and NH_3 on nitrate formation. Yang et al. (2017) carried out field observation with ACSM in Beijing for half a month and pointed out the importance of aerosol nitrate in haze formation. However, despite of an increasing number of studies using online techniques, continuous measurements with more than one-year period are still very limited.

The Yangtze River Delta (YRD) located in the eastern China, with megacities including Shanghai, Nanjing and Suzhou etc., has suffered from heavy particulate matter pollution and photochemical pollution (Ding et al., 2013bc; Wang et al., 2016bc; Wang et al., 2016a). Previous studies indicated an important role of nitrate in the pollution episodes (Hua et al., 2015; Du et al., 2011; Yang et al., 2017). For example, Zhang et al. (2015a) carried out an observation with ACSM in urban Nanjing during summer and autumn, and found nitrate and organic aerosols dominated the PM_1 composition. Shi et all. (2014) used MARGA instrument in Shanghai for months and found and increasing contribution of nitrate to PM_1 mass during pollution periods. Wang et al. (2016b) reported temporal variation and transport of $PM_{2.5}$ water soluble ions, including nitrate, in an urban site in Shanghai based on three-year continuous

measurement using MARGA. However, detailed investigation of the possible mechanisms governing nitrate behaviors during haze pollution is still rare.

In this study, we present a 2-year continuous measurement of particulate nitrate using MARGA at a rural site in Nanjing, a megacity in the western YRD region, with the target to get a comprehensive understanding of particulate nitrate behaviors and investigate the processes affecting nitrate in haze episodes. We first conducted general statistical analysis of particulate nitrate and characterized seasonal variation and diurnal pattern. A thermodynamic model was then applied to investigate the gas-particle partition of nitrate. The influence of air masses was also investigated by conducting backward Lagrangian dispersion modelling. Finally, we selected eighteen nitrate episodes and investigated the main processes influencing their evolution.

2. Methodology

2.1. Sample site and instrumentation

The SORPES station (118°57′E, 32°07′N) was located on the top of a small hill (40 m above sea level) in the Xianlin campus of Nanjing University located in the outskirts of Nanjing, China. The station is an ideal receptor of air masses from the YRD with little influence of local emissions and urban pollution from Nanjing. Detailed description can be found in previous studies (Ding et al., 2013c; Ding et al., 2016a).

The measurement was conducted from March 2014 to Feb 2016. Hourly concentrations of water soluble gases of HCl, HNO_3, HONO, SO_2 and NH_3, and water-soluble ions in $PM_{2.5}$, including Cl^-, NO_3^-, SO_4^{2-}, NH_4^+, Na^+, K^+, Ca^{2+}, and Mg^{2+}, were measured with a Monitor for Aerosols and Gases in ambient Air (MARGA, designed and manufactured by Applikon Analytical B.V., the Netherlands) employed in connection with a Thermo $PM_{2.5}$ cyclone inlet. The sampling system was comprised of two parts: A Wet Rotating Denuder for gases and a Steam Jet Aerosol Collector for aerosols, working at an air flow of 1 m^3 h^{-1} (ten Brink et al., 2007; Rumsey et al., 2014). After each hour's collection, the samples were analyzed using ion chromatography. The instrument was calibrated on an hourly basis using internal standard liquid (bromide

lithium), ensuring a stable and reliable ion chromatograph. Concentrations of all aerosol ions and gases have a precision of 0.001μg m^{-3} (Xie et al., 2015). The $PM_{2.5}$ ion dataset from the MARGA provided more than 15000 hourly samples over the 24 months of measurements considering points where NO_3^-, NH_4^+ and SO_4^{2-} were all available. Trace gases (i.e., O_3, SO_2, NO_x, NO) and $PM_{2.5}$ mass concentrations were also measured at SORPES (Ding et al., 2013c; Nie et al., 2015; Ding et al., 2016a), together with meteorological data including wind speed/direction, temperature, and relative humidity.

2.2. Thermodynamic constants and ISORROPIA II

Formation of ammonium nitrate involves an equilibrium reaction between the gas phase NH_3 and HNO_3, and particle phase NH_4NO_3. The gas-to-particle partitioning is temperature dependent, and the equilibrium constant can be calculated as follows (units $mol^2kg^{-2}atm^{-2}$) (Sun et al., 2011; Seinfeld and Pandis, 2006):

$$K=k_{298}\, exp(a(298/T-1) +b[1+ln(298/T)-298/T]) \quad (1)$$

$$K_{298}=3.5\times10^{16}(atm^{-2}),\ a=75.11,\ b=-13.5. \quad (2)$$

ISORROPIA II (available at http://isorropia.eas.gatech.edu/) is a thermodynamic model used commonly in inorganic aerosol research (Fountoukis and Nenes, 2007). To analyze gas-into-particulate pathway for nitrate formation, HNO_3 was modeled with ISORROPIA II run in forward model iteratively (Pusede et al., 2016; Fountoukis and Nenes, 2007). ISORROPIA II was initialized as $[NO_3^-+HNO_3]_{total} = [NO_3^-]_{aerosol}$. Calculated HNO_3(g) was added back to $[NO_3^-+HNO_3]$, while we always use $[NH_4^+{}_{aerosol}+NH_3(g)]$ as input total ammonium. ISORROPIA II was solved iteratively until output NO_3^- changed by < 2% by mass. The phase state was set as metastable. We assume that gases and aerosol are in equilibrium, that aerosols are homogeneous and internally mixed, and that unaccounted-for factors do not influence the thermodynamics of system (Vayenas et al., 2005).

2.3. Lagrangian Dispersion Modeling

To help understand the influence of air masses, backward Lagrangian particulate dispersion modeling (LPDM) was carried out based on a method developed and

evaluated by Ding (Ding et al., 2013a). The LPDM was conducted using the Hybrid Single-Particulate Lagrangian Integrated Trajectory model developed in the Air Resource Laboratory (ARL) of the National Oceanic and Atmospheric Administration using the ARL format Global Data Assimilation System data. The model calculates the position of particulates by mean wind and a turbulence transport component after they are released at the source point for a backward simulation. For each hour, 3000 particulates were released at 100 m altitude over the site and were traced backward for a 3-day period. The hourly position of each particulate was calculated using a 3-D particulate, i.e., horizontal and vertical, method. The residence time at 100 m altitude, i.e., foot-print "retroplume", which represents the distribution of the surface probability or residence time of the simulated air mass, was used to understand the contribution from potential source regions (Ding et al., 2013ac; Shen et al., 2018).

2.4. Steady-state predictions

Based on their short lifetimes, the concentrations of the NO_3 radical and N_2O_5 can be predicted by steady-state calculations due to lack of measurement data (Osthoff et al., 2006). The formation and loss of N_2O_5 associated with a series of chemical reactions are listed in Table 1. For the heterogeneous processes, we used 0.004 and 0.03 as the uptake coefficients of the NO_3 radical and N_2O_5 (γNO_3 and γN_2O_5), respectively (Aldener et al., 2006; Wen et al., 2015; Knopf et al., 2011; Brown et al., 2006). Due to the lack of measurement during 2014 - 2016, the VOCs data used here was the average of nighttime value that measured at SORPES station during the wintertime of 2017. The corresponding rate constant can be found in Master Chemical Mechanism (MCM version 3.1, http://mcm.leeds.ac.uk/MCM/). The uncertainty that caused by the limited VOCs measurements and the variation of N_2O_5 uptake coefficient were estimated and discussed in the supplement.

3. Results and discussion

3.1. Overall results

A MARGA was deployed to continuously measure the eight water-soluble ions (WSI)

of $PM_{2.5}$ and several gas-phase species from March 2014 to February 2016 with the time resolution of 1-hour. Nitrate (NO_3^-), sulfate (SO_4^{2-}) and ammonium (NH_4^+) were the major components with the two-year averaged concentrations of 15.8 (±13.4),15.3 (±10.6) and 10.4 (±7.6) μg m^{-3}, respectively. In the present study, we focused on nitrate, and discussed the temporal variation and its association with physicochemical processes. The concentration of $PM_{2.5}$ nitrate changed largely from 0.5 to 92.6 μg m^{-3} during the measurement period, and accounted for 3% to 58% of total WSI (=45.7 + 30μg m^{-3}). The highest hourly nitrate concentration occurred on December 23, 2015 together with high concentrations of sulfate (65.5 μg m^{-3}), and ammonium (56.8 μg m^{-3}). Heavy haze episode like this occurred at our site frequently during winter. To understand the influence of wind on nitrate concentration, the wind rose plot is given in Fig. S2. The prevailing winds at the SORPES station were from northeast and east during the two-year observation period. Particulate nitrate tended to accumulate or formed under stagnant condition of low wind speed. The wind from west and east can lead to a higher nitrate concentration and also other aerosol components (Ding et al., 2013bc; Shen et al., 2018), which may be associated with air masses from biomass burning region and the city clusters of YRD.

To get an overall picture of nitrate distribution in developed region of costal China, we reviewed results from available nitrate measurements in three most polluted regions of North China Plain (NCP), YRD and Pearl River Delta (PRD), and summarized their concentration, sampling sites and measurement techniques in Fig.1. The corresponding data and references are listed in table S2. Measurements in summer and winter were separated due to the large seasonal difference of particulate nitrate. Despite that these measurements were from various measurement techniques, the results still can give us some insights about the differences in spatial and temporal scales. First, particulate nitrate generally showed the highest concentration in NCP and followed by YRD and PRD. This was in consistence with the spatial distribution of NO_2 – a major gas precursor of nitrate. Second, evident seasonal variations can be observed at all three

regions with much higher concentrations in winter. Third, an overall increase of particulate nitrate was implied in NCP and YRD in the past decade, especially that during summertime (shown in Fig.1a). Nevertheless, particulate nitrate in PRD revealed an overall decreasing trend. It should be noted that the dataset cited in Fig. 1 were obtained from different sites with different techniques. Trends inferred from these datasets could suffer from considerable uncertainty. Compared to these previous studies, the nitrate concentration during summertime at SORPES station was lower than that in NCP, but higher than that in YRD and PRD cities. In terms of wintertime, nitrate concentration at SORPES station was slightly lower than that in NCP, comparable with that in YRD, and higher than that in PRD.

Fig. 2 illustrates the occurrence frequency of the loading of particle matter in different concentration ranges, and the changes of nitrate proportion along with the PM loading. Noting that the PM loading here was indicated by the mass of total WSI. The highest frequency of WSI concentrations occurred in a range of 20-40 μg m^{-3}, and gradually decreased with the increasing of concentration. Heavy PM pollution with WSI concentrations higher than 100 μg m^{-3} occurred during more than 5% of the time during this study. The contribution of nitrate to total WSI increased with the PM loading, ranging from ~25% with WSI concentration lower than 20 μg m^{-3} to ~ 40% when WSI was higher than 140 μg m^{-3}. These results suggested that nitrate was a major driver of haze episodes with high PM peaks in this region.

Fig. 3a shows the scatter plot of particulate nitrate and total WSI. The correlation coefficient was 0.92 and nitrate accounted for 32% of the total WSI. Air temperature greatly affected the contribution of nitrate to total WSI. Its proportion can be up to 58% at in the temperature range of 0 °C to 5 °C and only 3% at the temperature higher than 30 °C, indicating an important role of thermodynamic equilibrium in nitrate concentration. We further investigated the neutralization extent of sulfate and nitrate by ammonium (Fig. 3b). Ammonium was overall enough to neutralize both sulfate and nitrate, suggesting that the particulate nitrate mostly existed as ammonium nitrate at

SORPES station. This is different from the ammonia poor regions, where the uptake of HNO_3 to dust/sea salt particles was found to be important to $PM_{2.5}$ nitrate (Griffith et al., 2015). Seasonal difference can be observed for the molar ratio of ammonium to the sum of sulfate and nitrate. In spring and early summer, a fraction of the particulate nitrate is present as $Ca(NO_3)_2$ and KNO_3, which could explain the data points below the regression line in Fig. 3b. In winter, considerable ammonium is existed as NH_4Cl (Hu et al., 2017), resulting in the data points above the regression line.

3.2. Characteristics of fine particular nitrate in different seasons.

3.2.1. Seasonal pattern and its main causes

Fig. 4 shows the composite seasonal pattern of NO_x, $PM_{2.5}$ nitrate, sulfate and the molar-based ratio of nitrate to sulfate during the 2-year period at SORPES station. The seasonal variations of other related species and nitrate-to-$PM_{2.5}$-ratio are shown in Table S3. Similar to the previous studies (Griffith et al., 2015), a typical seasonal variation was observed for particulate nitrate (and its ratio to sulfate, i.e. NO_3^-/SO_4^{2-}), with a maximum value of 23.7 μg m^{-3} (140%) in January, and a minimum of 8.4 μg m^{-3} (66%) in August and September. Particulate sulfate exhibits a relatively less pronounced seasonal pattern with a small peak in June. The low value of particulate nitrate during summer can be generally explained by the higher temperature, higher and unstable boundary layer and relative clean air masses induced by summer monsoon (Ding et al., 2013c) despite of the increased photochemical formation. In opposite, the high values during winter were generally due to the lower temperature, lower and stable boundary layer and relative stronger continental outflow from the North China where anthropogenic emission was relatively high due to heating in winter (Ding et al., 2013c). Different chemical processes that affects nitrate concentrations between summer and winter will be discussed later. NO_x, the major precursor, tracked the changes of particulate nitrate, except for that during February and June. In addition, a secondary peak of particulate nitrate can be observed during June, which can be explained as the influence from agricultural burning in eastern China (Ding et al., 2013bc; Xie et al.,

2015; Shen et al., 2018). The concentrations of Potassium, a biomass burning tracer in this region (Ding et al., 2013b; Xie et al., 2015), clearly showed a consistent peak (Fig. S3) with both particulate nitrate and sulfate, as well as the discrepancy of NO_x and nitrate concentrations (Ding et al., 2013b; Xie et al., 2015; Nie et al., 2015) shown in Fig. 4. While in February, the nitrate concentration didn't show concurrent decrease in NO_x during the Chinese Spring Festival (Ding et al., 2013c). The observations might suggest that particulate nitrate is influenced by regional transport but not the local emissions in February.

3.2.2. Diurnal cycles during summer and winter

In Fig. 5, we show the averaged diurnal variations of particulate nitrate, nitrogen dioxide, nitric acid, equilibrium constant (*K*), air temperature and RH during summer and winter during the two years. Nitric acid was calculated by ISORROPIA II. In summer (Fig. 5a), the fine particulate nitrate showed a typical diurnal cycle that the maximum concentration occurred at 7:00 with the average concentration of 16.5 μg m^{-3} and minimum value at 14:00 (7.2 μg m^{-3}). This summertime diurnal pattern of nitrate is very similar with the findings in Shandong (Wen et al., 2015) and New York (Sun et al., 2011). However, it is quite different from the findings in Hong Kong (Griffith et al., 2015), where nitrate concentration peaks in the daytime in summer. Ambient temperature and the development of boundary layer are the major drivers to the observed diurnal variation of particulate nitrate, and high temperature and high boundary layer during daytime lead to evaporation and dilution of the particulate nitrate (Zhang et al., 2015a; Ding et al., 2016). Nitric acid, which accounted for 20% of the total nitrate [NO_3^-+HNO_3], revealed its high concentration (around 2 ppb) in the noontime (12:00-15:00). NO_2, the precursor of nitrate, showed a peak concentration of 18.2 ppb at 21:00, and remained at a high level during the whole night. The Equilibrium constant, *K*, was calculated to understand the influence of gas-to-particulate partitioning on the observed diurnal variation of particulate nitrate (Sun et al., 2011). As showed in Fig. 5a, *K* showed the same diurnal pattern as particulate nitrate, suggesting the

thermodynamic is the major factor influencing the diurnal variation of particle nitrate during summer.

In winter, the diurnal variation is small with a moderate peak at around 10:00 AM. Compared to that in summer, K showed similar diurnal variation, but not correlated to particulate nitrate, indicating factors other than the control of temperature. The observed peak at late morning was probably due to downward mixing from the residual layer where particulate nitrate was formed aloft during the night and brought to the surface after sunrise following the breakup of the boundary layer (Baasandorj et al., 2017; Young et al., 2016; Pusede et al., 2016). Direct vertical observations are needed to further investigate this issue.

To further investigate factors influencing the nitrate behaviors other than thermodynamics, ISORROPIA II was used to simulate the diurnal variation of nitrate. Hourly concentrations of all species (both gas and aerosol phase species) at 00:00 were used as the initial value of each specific day. Hourly data of temperature and relative humidity were used as the input data to constrain the model. The ISORROPIA II model was set as forward mode and metastable phase state. The calculated diurnal variations are shown in Fig. 6 together with the observed results.

The differences between the calculation and the observation could be attributed to: (1) the development of boundary layer, (2) the dry deposition of nitric acid, and (3) chemical processes, which has not been considered yet in the model. As shown in Fig. 6a, the overall diurnal pattern of nitrate in summer is well captured by the model except for 3 periods. The differences after midnight are likely caused by the effect of boundary layer height and some chemical processes. Faster increase of model nitrate after 18:00 was attributed to lack of dry deposition of nitric acid in the model. During noontime the observed nitrate concentration was expected to be lower than the calculated value because of the development of boundary layer and stronger dry deposition of nitric acid associated with stronger turbulence mixing, which were neglected in the model. However, in contrast, the observation was considerably higher than the calculated value.

It indicates a strong production of nitrate via photochemical processes in summer. Fig.6c shows that the difference between calculated and observed nitrate concentration was in good correlation with the product of NO_2 and solar radiation, a proxy for the production rate of nitric acid (Zhang et al., 2005; Young et al., 2016), further suggesting that photo-oxidation of NO_2 is an important source of nitrate during summer, even though the thermodynamic equilibrium is the dominate factor controlling the diurnal cycle. Wen et al. (2018) also demonstrated that photochemical production of nitric acid is a major contributor to daytime nitrate increase during summer in North China Plain. In winter, the influence of thermodynamics on diurnal cycle is small since the relatively low temperature throughout the day. The peaks in the morning may be caused by the mixing down of a residual layer enriched of nitrate as mentioned above, while the decline during the afternoon are supposed to be the result of dilution associated with the boundary layer development.

3.2.3 Influence of air masses transport

Meteorological processes play a key role in air masses long-range transport and local accumulation (Ding et al., 2013ac; Zhang et al., 2016; Ding et al, 2016b). In order to investigate the influence of air masses transport on nitrate concentrations, Lagrangian dispersion modeling was conducted for the sampling days with the top and bottom 25% nitrate concentration in summer and winter, respectively (Ding et al., 2013a). Fig. 7 shows the retroplumes, i.e. footprint at an altitude of 100 m, of the selected days during summer and winter, respectively. In summer, high concentrations of nitrate tended to be associated with the air masses from west of Nanjing (mostly Anhui province) and Yangtze River Delta (Suzhou-Shanghai city clusters and North Zhejiang province) (Fig. 7a). YRD is a high NO_x emission region (Fig. 1), air masses from which could bring high concentration of NO_x to enhance the nitrate concentration at SORPES station. Biomass burning is the possible cause of the high nitrate loading with air mass from the west of Nanjing (Fig. S4). In winter, regional transport from northern China played an important role in enhancing nitrate concentrations. As shown in Fig. 8c, a large part of

air masses for the highest 25% sampling days was from North China Plain, which has the strongest NO_x emission in China (Fig. 1). It should be noted here that the longer lifetime of particulate nitrate during winter might be the main cause to promote the contribution of regional transport to the observed nitrate at SORPES. In contrast, the lowest 25% sampling days during winter tended to be accompanied with the air mass from Nanjing local and marine areas.

3.3. Contribution of N_2O_5 hydrolysis to nitrate episodes

Similar to findings from previous studies (Zhang et al., 2015c), nitrate was found to increase significantly during this study and become the largest contributor of $PM_{2.5}$ during the haze episodes (Fig. 2). Generally, these pollution episodes mainly occurred in winter (Fig. 3a and Fig. 4), during which the photochemical production of nitric acid should be weak. N_2O_5 hydrolysis was thus proposed to be a potential important formation pathway. Here we investigated the nitrate episodes in detail and discussed their relationship to the N_2O_5 hydrolysis during the nights before.

In Fig. 8, we show a typical case of nitrate episodes from 30 November to 2 December, 2015. Fast nitrate formation was observed, which was likely caused by hydrolysis of N_2O_5. Nitrate increased significantly from 20.3 μg m^{-3} at 18:00 of 30 November to 63 μg m^{-3} at 6:00 of 1 December, 2015. The ratio of nitrate to $PM_{2.5}$ also exhibited a large increase from 25% at 18:00 to 38% at 06:00. In contrast, other $PM_{2.5}$ components, e.g. sulfate and black carbon, showed only slight increases. High concentration of NO_2, considerable level of O_3 and extremely low concentration of NO provided a favorable condition towards forming NO_3 and N_2O_5 (Brown et al., 2003). The meteorological conditions during these 12 hours were stable with low wind speed and high relative humidity, which, combined with the relatively high concentration of PM, would promote the hydrolysis of N_2O_5 (Riemer, 2003).

N_2O_5 concentrations were calculated by using the steady-state approximation (Osthoff et al., 2006;Wang et al., 2014;Wen et al., 2015), and the result was shown in Fig. 8. The calculated N_2O_5 exhibited a much higher concentration during the night of

30 November compared to the days before and after. Particulate nitrate formed from N_2O_5 hydrolysis was then computed during the 12-hour period. Nitrate concentration at 18:00 of 30 November, 2015 (20 μg m^{-3}) was selected as the initial value, and 31 μg m^{-3} of particulate nitrate was produced in the following 12 hours, suggesting that approximate 80% of increased particulate nitrate can be attributed to the hydrolysis of N_2O_5 in this case.

To further understand the contribution of N_2O_5 hydrolysis, sampling days with daily-averaged nitrate concentration exceeding the mean plus twice the standard deviation were selected as the nitrate episode days. In total, 18 episode-days were selected during the 2-year measurement, with 16 days in winter and the other 2 days in biomass burning season. In Fig. 9, we presented the averaged diurnal pattern of particulate nitrate and its related parameters on the 18 selected episode and pre-episode days. For the episode days, particulate nitrate revealed a similar diurnal pattern as that of the whole winter (Fig. 5). Nitrate maintained a high concentration during the whole day with a small peak around 10:00 in the morning. However, for the pre-episode days, a clear build-up of nitrate can be observed, especially during the nighttime from 17:00 of the pre-episode days to 1:00 of the episode days (as marked in Fig. 9). The average increment of ammonium nitrate exceeded 24 μg m^{-3} during this 9-hour period of the pre-episode nighttime. The total WIS also increased during this period, which was mostly attributed to ammonium nitrate (almost 90%) and resulted in an evident increase of the ratio of nitrate to total WSI. Compared to nitrate, black carbon, a tracer of primary emissions, showed little change during the pre-episode day. The retroplume showed in Fig. S5 suggested that the air masses arrived at the SORPES station on the pre-episode and episode days were almost the same. These results suggest that secondary formation other than accumulation was the major contributor to the observed increase of particulate nitrate.

Since the observed nitrate formation mostly occurred during the nighttime of pre-episode days when the photochemical production of nitric acid would be largely

suppressed, N_2O_5 hydrolysis is thus believed to be the major contributor. As showed in Fig. 9, compared to those during episode days, NO_2 concentration was comparable with the average concentrations of 28 ppb, the but O_3 concentration was higher during pre-episode days. This resulted in a higher production rate of N_2O_5 proxy (PNO_3) in pre-episode days, and favored formation of nitrate from the hydrolysis of N_2O_5. We further calculated the contribution of N_2O_5 hydrolysis to nitrate formation during the periods from 17:00 to 23:00 of each pre-episode day (excluding 2 windy days). A good correlation (R=0.8) was observed between the calculated nitrate and observed nitrate (Fig. 10), with the slope of 0.77, indicating the observed nitrate formation during nitrate episodes were significantly attributed to the hydrolysis of N_2O_5. It should be noted that this calculation suffered from considerable uncertainties due to the variability of actual VOCs concentrations and N_2O_5 uptake coefficient. The detailed uncertainty calculation is discussed in the supplement (Fig. S1).

4. Summary and Conclusion

Online measurements of fine particulate nitrate along with trace gases and $PM_{2.5}$ mass concentrations were conducted for two years from March 2014 to February 2016 using a MARGA at SORPES station, a rural receptor site in the Yangtze River Delta, eastern China. Hourly nitrate concentration varied from 0.5 μg m^{-3} to 92.6 μg m^{-3}, with an averaged value of 15.8 μg m^{-3}, which was generally higher than the measurement at the sites in YRD and PRD, but lower than that at the sites in North China Plain. The contribution of nitrate to total WSI increased from 25% with WSI concentration lower than 20 μg m^{-3}, to 40% when WSI was higher than 140 μg m^{-3}, suggesting a major driver of nitrate to the aerosol pollution in YRD. NH_3 is enough to neutralize the acidic compounds of aerosol, and ammonium nitrate was thus the predominate form of the observed particulate nitrate. A clear seasonal variation of nitrate was observed with peak value in January and December and lowest value in August and September. Biomass burning plumes contributed to the nitrate concentration evidently and resulted in a secondary peak during June. In summer, thermodynamic equilibrium was the major

449 factor influencing the diurnal variation of nitrate, and resulted in a much lower
450 concentration at noontime. Nevertheless, the observed nitrate at noontime was
451 considerably higher than the value predicted by the ISORROPIA II model, indicating a
452 strong production of nitrate by the photo-oxidation of NO_2. Air masses from YRD and
453 the biomass burning region were associated with the high nitrate concentrations during
454 summer. In winter, the diurnal variation of nitrate was weak. Regional transport from
455 the North China Plain contributed largely to the observed high nitrate concentrations.
456 Nitrate episodes, defined as daily-averaged concentration exceeding the mean
457 value plus twice the standard deviation, were further investigated to understand the
458 chemical processes towards forming particulate nitrate and their contribution to the
459 pollution episodes. A clear build-up of nitrate can be observed during the pre-episode
460 night, which dominated the increase of total WSI. N_2O_5 hydrolysis was demonstrated
461 to contribute 80% of the observed nitrate formation, suggesting its critical role in an
462 aerosol pollution episode. In view of the significant emission of NO, which is the main
463 sink of N_2O_5 during night, stronger production of N_2O_5 is expected at the upper
464 boundary layer, e.g. residual layer, and this residual layer N_2O_5 will contribute to the
465 nitrate formation in the entire boundary layer. In summary, our study provides evidence
466 that particulate nitrate especially that formed from N_2O_5 hydrolysis is a crucial
467 contributor to the aerosol pollution episodes in eastern China.

468 *Data availability.* The GDAS data used in the HYSPLIT calculation can be acquired
469 from ftp://arlftp.arlhq.noaa.gov/pub/archives/gdas1. Measurement data at SORPES,
470 including aerosol data and relevant trace gases as well as meteorological data, are
471 available upon request from the corresponding author before the SORPES database is
472 opened publicly.

473 *Acknowledgements.* The research was supported by National Key Research &
474 Development Program of China (2016YFC0200500) and National Science Foundation

of China (41725020， 91544231, 91644218, 41422504, 91744311, 41675145).

References

Aldener, M., Brown, S. S., Stark, H., Williams, E. J., Lerner, B. M., Kuster, W. C., Goldan, P. D., Quinn, P. K., Bates, T. S., Fehsenfeld, F. C., and Ravishankara, A. R.: Reactivity and loss mechanisms of NO3 and N2O5 in a polluted marine environment: Results from in situ measurements during New England Air Quality Study 2002, J Geophys Res-Atmos, 111, 2006.

Baasandorj, M., Hoch, S. W., Bares, R., Lin, J. C., Brown, S. S., Millet, D. B., Martin, R., Kelly, K., Zarzana, K. J., Whiteman, C. D., Dube, W. P., Tonnesen, G., Jaramillo, I. C., and Sohl, J.: Coupling between Chemical and Meteorological Processes under Persistent Cold-Air Pool Conditions: Evolution of Wintertime PM2.5 Pollution Events and N2O5 Observations in Utah's Salt Lake Valley, Environ Sci Technol, 51, 5941-5950, 10.1021/acs.est.6b06603, 2017.

Bian, Q., Huang, X. H. H., and Yu, J. Z.: One-year observations of size distribution characteristics of major aerosol constituents at a coastal receptor site in Hong Kong – Part 1: Inorganic ions and oxalate, Atmospheric Chemistry and Physics, 14, 9013-9027, 10.5194/acp-14-9013-2014, 2014.

Brown, S. S., Stark, H., Ryerson, T. B., Williams, E. J., Nicks, D. K., Trainer, M., Fehsenfeld, F. C., and Ravishankara, A. R.: Nitrogen oxides in the nocturnal boundary layer: Simultaneous in situ measurements of NO3, N2O5, NO2, NO, and O-3, J Geophys Res-Atmos, 108, 2003.

Brown, S. S., Ryerson, T. B., Wollny, A. G., Brock, C. A., Peltier, R., Sullivan, A. P., Weber, R. J., Dube, W. P., Trainer, M., Meagher, J. F., Fehsenfeld, F. C., and Ravishankara, A. R.: Variability in nocturnal nitrogen oxide processing and its role in regional air quality, Science, 311, 67-70, 2006.

Brown, S. S., and W.P.Dube.: High resolution vertical distributions of NO_3 and N_2O_5 through the nocturnal boundary layer, Atmospheric Chemistry and Physics, 7, 139-149, 2007.

Brown, S. S., and Stutz, J.: Nighttime radical observations and chemistry, Chem Soc Rev, 41, 6405-6447, 2012.

Brown, S. S., Dube, W. P., Tham, Y. J., Zha, Q. Z., Xue, L. K., Poon, S., Wang, Z., Blake, D. R., Tsui, W., Parrish, D. D., and Wang, T.: Nighttime chemistry at a high altitude site above Hong Kong, J Geophys Res-Atmos, 121, 2457-2475, 10.1002/2015JD024566, 2016.

Calvert, J. G., and Stockwell, W. R.: Acidic generation in the troposphere by gas phase chemistry, Environ. Sci. Technol., 17, 428-443, 1983.

Cao, J.-J., Shen, Z.-X., Chow, J. C., Watson, J. G., Lee, S.-C., Tie, X.-X., Ho, K.-F., Wang, G.-H., and Han, Y.-M.: Winter and Summer PM2.5 Chemical Compositions in Fourteen Chinese Cities, Journal of the Air & Waste Management Association, 62, 1214-1226, 10.1080/10962247.2012.701193, 2012.

Charlson, R., and Heintzenberg, J.: Aerosol Forcing of Climate Environmental Sciences Research Report, 1995.

Ding, A., Wang, T., and Fu, C.: Transport characteristics and origins of carbon monoxide and ozone in Hong Kong, South China, Journal of Geophysical Research: Atmospheres, 118, 9475-9488, 10.1002/jgrd.50714, 2013a.

Ding, A. J., Fu, C. B., Yang, X. Q., Sun, J. N., Petäjä, T., Kerminen, V. M., Wang, T., Xie, Y., Herrmann, E., Zheng, L. F., Nie, W., Liu, Q., Wei, X. L., and Kulmala, M.: Intense atmospheric pollution modifies weather: a case of mixed biomass burning with fossil fuel combustion pollution in eastern China, Atmospheric Chemistry and Physics, 13, 10545-10554, 10.5194/acp-13-10545-2013, 2013b.

Ding, A. J., Fu, C. B., Yang, X. Q., Sun, J. N., Zheng, L. F., Xie, Y. N., Herrmann, E., Nie, W., Petäjä, T., Kerminen, V. M., and Kulmala, M.: Ozone and fine particle in the western Yangtze River Delta: an overview of 1 yr data at the SORPES station, Atmospheric Chemistry and Physics, 13, 5813-5830, 10.5194/acp-13-5813-2013, 2013c.

Ding, A.J., Nie, W., Huang, X., Chi, X., Sun, J., Kerminen,V.-M., Xu, Z., Guo, W., Petäjä, T., Yang, X., Kulmala, M., and Fu, C.: Long-term observation of air pollution-weather/climate interactions at the SORPES station: a review and outlook, Front. Environ. Sci. & Eng., 10, 5, 15, 2016a.

Ding, A.J., Huang, X., Nie, W., Sun, J.N., Kerminen, V.-M., Petaja, T., Su, H., Cheng, Y.F., Yang, X.-Q., Wang, M.H., Chi, X.G., Wang, J.P., Virkkula, A., Guo, W.D., Yuan, J., Wang, S.Y., Zhang, R.J., Wu, Y.F., Song, Y., Zhu, T., Zilitinkevich, S., Kulmala, M., and Fu, C.B.: Ehanced haze pollution by black carbon in megacities in China, Geophys. Res. Lett., 43, 6, 2873-2879, 2016b.

Du, H., Kong, L., Cheng, T., Chen, J., Du, J., Li, L., Xia, X., Leng, C., and Huang, G.: Insights into summertime haze pollution events over Shanghai based on online water-soluble ionic composition of aerosols, Atmospheric Environment, 45, 5131-5137, 10.1016/j.atmosenv.2011.06.027, 2011.

Fountoukis, C., and Nenes, A.: ISORROPIA II: a computationally efficient thermodynamic equilibrium model for K+-Ca2+-Mg2+-Nh(4)(+)-Na+-SO42--NO3--Cl--H2O aerosols, Atmospheric Chemistry and Physics, 7, 4639-4659, 2007.

Gao, X. M., Yang, L. X., Cheng, S. H., Gao, R., Zhou, Y., Xue, L. K., Shou, Y. P., Wang, J., Wang, X. F., Nie, W., Xu, P. J., and Wang, W. X.: Semi-continuous measurement of water-soluble ions in PM2.5 in Jinan, China: Temporal variations and source apportionments, Atmospheric Environment, 45, 6048-6056, 2011.

Griffith, S. M., Huang, X. H. H., Louie, P. K. K., and Yu, J. Z.: Characterizing the thermodynamic and chemical composition factors controlling PM2.5 nitrate: Insights gained from two years of online measurements in Hong Kong, Atmospheric Environment, 122, 864-875, 10.1016/j.atmosenv.2015.02.009, 2015.

He, L.-Y., Huang, X.-F., Xue, L., Hu, M., Lin, Y., Zheng, J., Zhang, R., and Zhang, Y.-H.: Submicron aerosol analysis and organic source apportionment in an urban atmosphere in Pearl River Delta of China using high-resolution aerosol mass spectrometry, Journal of Geophysical Research, 116, 10.1029/2010jd014566, 2011.

Hu, W., Hu, M., Hu, W.-W., Zheng, J., Chen, C., Wu, Y., and Guo, S.: Seasonal variations in high time-

resolved chemical compositions, sources, and evolution of atmospheric submicron aerosols in the megacity Beijing, Atmospheric Chemistry and Physics, 17, 9979-10000, 10.5194/acp-17-9979-2017, 2017.

Hua, Y., Cheng, Z., Wang, S., Jiang, J., Chen, D., Cai, S., Fu, X., Fu, Q., Chen, C., Xu, B., and Yu, J.: Characteristics and source apportionment of PM2.5 during a fall heavy haze episode in the Yangtze River Delta of China, Atmospheric Environment, 123, 380-391, 10.1016/j.atmosenv.2015.03.046, 2015.

John, W., Wall, S. M., and Ondo, J. L.: A New Method for Nitric-Acid and Nitrate Aerosol Measurement Using the Dichotomous Sampler, Atmospheric Environment, 22, 1627-1635, 1988.

Knopf, D. A., Forrester, S. M., and Slade, J. H.: Heterogeneous oxidation kinetics of organic biomass burning aerosol surrogates by O-3, NO2, N2O5, and NO3, Phys Chem Chem Phys, 13, 21050-21062, 2011

Lei, H., and Wuebbles, D. J.: Chemical competition in nitrate and sulfate formations and its effect on air quality, Atmospheric Environment, 80, 472-477, 10.1016/j.atmosenv.2013.08.036, 2013.

Li, H., Zhang, Q., Zhang, Q., Chen, C., Wang, L., Wei, Z., Zhou, S., Parworth, C., Zheng, B., Canonaco, F., Prévôt, A. S. H., Chen, P., Zhang, H., Wallington, T. J., and He, K.: Wintertime aerosol chemistry and haze evolution in an extremely polluted city of the North China Plain: significant contribution from coal and biomass combustion, Atmospheric Chemistry and Physics, 17, 4751-4768, 10.5194/acp-17-4751-2017, 2017.

Nie, W., Wang, T., Gao, X., Pathak, R. K., Wang, X., Gao, R., Zhang, Q., Yang, L., and Wang, W.: Comparison among filter-based, impactor-based and continuous techniques for measuring atmospheric fine sulfate and nitrate, Atmospheric Environment, 44, 4396-4403, 10.1016/j.atmosenv.2010.07.047, 2010.

Nie, W., Ding, A. J., Xie, Y. N., Xu, Z., Mao, H., Kerminen, V. M., Zheng, L. F., Qi, X. M., Huang, X., Yang, X. Q., Sun, J. N., Herrmann, E., Petäjä, T., Kulmala, M., and Fu, C. B.: Influence of biomass burning plumes on HONO chemistry in eastern China, Atmospheric Chemistry and Physics, 15, 1147-1159, 10.5194/acp-15-1147-2015, 2015.

Osthoff, H. D., Sommariva, R., Baynard, T., Pettersson, A., Williams, E. J., Lerner, B. M., Roberts, J. M., Stark, H., Goldan, P. D., Kuster, W. C., Bates, T. S., Coffman, D., Ravishankara, A. R., and Brown, S. S.: Observation of daytime N2O5in the marine boundary layer during New England Air Quality Study-Intercontinental Transport and Chemical Transformation 2004, Journal of Geophysical Research: Atmospheres, 111, n/a-n/a, 10.1029/2006jd007593, 2006.

Pathak, R. K., and W.S.Wu: Summertime PM2.5 ionic species in four major cities of China; nitrate formation in an ammonia-deficient atmosphere, Atmospheric Chemistry and Physics, 9, 1711-1722, 2009.

Pathak, R. K., Wang, T., and Wu, W. S.: Nighttime enhancement of PM2.5 nitrate in ammonia-poor atmospheric conditions in Beijing and Shanghai: Plausible contributions of heterogeneous

hydrolysis of N2O5 and HNO3 partitioning, Atmospheric Environment, 45, 1183-1191, 10.1016/j.atmosenv.2010.09.003, 2011.

Petetin, H., Sciare, J., Bressi, M., Gros, V., Rosso, A., Sanchez, O., Sarda-Estève, R., Petit, J.-E., and Beekmann, M.: Assessing the ammonium nitrate formation regime in the Paris megacity and its representation in the CHIMERE model, Atmospheric Chemistry and Physics, 16, 10419-10440, 10.5194/acp-16-10419-2016, 2016.

Pusede, S. E., Duffey, K. C., Shusterman, A. A., Saleh, A., Laughner, J. L., Wooldridge, P. J., Zhang, Q., Parworth, C. L., Kim, H., Capps, S. L., Valin, L. C., Cappa, C. D., Fried, A., Walega, J., Nowak, J. B., Weinheimer, A. J., Hoff, R. M., Berkoff, T. A., Beyersdorf, A. J., Olson, J., Crawford, J. H., and Cohen, R. C.: On the effectiveness of nitrogen oxide reductions as a control over ammonium nitrate aerosol, Atmospheric Chemistry and Physics, 16, 2575-2596, 10.5194/acp-16-2575-2016, 2016.

Riemer, N.: Impact of the heterogeneous hydrolysis of N2O5on chemistry and nitrate aerosol formation in the lower troposphere under photosmog conditions, Journal of Geophysical Research, 108, 10.1029/2002jd002436, 2003.

Rumsey, I. C., Cowen, K. A., Walker, J. T., Kelly, T. J., Hanft, E. A., Mishoe, K., Rogers, C., Proost, R., Beachley, G. M., Lear, G., Frelink, T., and Otjes, R. P.: An assessment of the performance of the Monitor for AeRosols and GAses in ambient air (MARGA): a semi-continuous method for soluble compounds, Atmospheric Chemistry and Physics, 14, 5639-5658, 10.5194/acp-14-5639-2014, 2014.

Seinfeld, J. H., and Pandis, S. N.: Atmospheric Chemistry and Physics: From Air Pollution to Climate Change, John Wiley & Sons, New York, 2nd edition, 1232 pp., 13: 978-0-471-72018-8 2006.

Sharma, M., Kishore, S., Tripathi, S. N., and Behera, S. N.: Role of atmospheric ammonia in the formation of inorganic secondary particulate matter: A study at Kanpur, India, Journal of Atmospheric Chemistry, 58, 1-17, 10.1007/s10874-007-9074-x, 2007.

Shen, Y., Virkkula, A., Ding, A., Wang, J., Chi, X., Nie W., Qi, X., Huang, X., Liu Q., Zheng, L., Xu, Z., Petaja, T., Aalto, P.P., Fu, C. and Kulmala, M.: Aerosol optical properties at SORPES in Nanjing, East China, Atmos. Chem. Phys., 18, 5265-5292, 2018.

Shi, Y., Chen, J., Hu, D., Wang, L., Yang, X., and Wang, X.: Airborne submicron particulate (PM1) pollution in Shanghai, China: chemical variability, formation/dissociation of associated semi-volatile components and the impacts on visibility, The Science of the total environment, 473-474, 199-206, 10.1016/j.scitotenv.2013.12.024, 2014.

Sun, Y. L., Zhang, Q., Schwab, J. J., Demerjian, K. L., Chen, W. N., Bae, M. S., Hung, H. M., Hogrefe, O., Frank, B., Rattigan, O. V., and Lin, Y. C.: Characterization of the sources and processes of organic and inorganic aerosols in New York city with a high-resolution time-of-flight aerosol mass apectrometer, Atmospheric Chemistry and Physics, 11, 1581-1602, 10.5194/acp-11-1581-2011, 2011.

ten Brink, H., Otjes, R., Jongejan, P., and Slanina, S.: An instrument for semi-continuous monitoring of the size-distribution of nitrate, ammonium, sulphate and chloride in aerosol, Atmospheric

Environment, 41, 2768-2779, 10.1016/j.atmosenv.2006.11.041, 2007.

Thornton, J. A., Braban, C. F., and Abbatt, J. P. D.: N2O5 hydrolysis on sub-micron organic aerosols: the effect of relative humidity, particle phase, and particle size, Phys Chem Chem Phys, 5, 4593-4603, 2003

van der A, R. J., Mijling, B., Ding, J., Koukouli, M. E., Liu, F., Li, Q., Mao, H., and Theys, N.: Cleaning up the air: effectiveness of air quality policy for SO2 and NOx emissions in China, Atmospheric Chemistry and Physics, 17, 1775-1789, 10.5194/acp-17-1775-2017, 2017.

Vayenas, D. V., Takahama, S., Davidson, C. I., and Pandis, S. N.: Simulation of the thermodynamics and removal processes in the sulfate-ammonia-nitric acid system during winter: Implications for PM2.5 control strategies, J Geophys Res-Atmos, 110, 2005.

Wang, D., Zhou, B., Fu, Q., Zhao, Q., Zhang, Q., Chen, J., Yang, X., Duan, Y., and Li, J.: Intense secondary aerosol formation due to strong atmospheric photochemical reactions in summer: observations at a rural site in eastern Yangtze River Delta of China, The Science of the total environment, 571, 1454-1466, 10.1016/j.scitotenv.2016.06.212, 2016a.

Wang, H.L., Qiao, L.P., Lou S.R., Zhou, M., Ding, A.J., Huang, H.Y., Chen, J.M., Wang, Q., Tao, S.K., Chen, C.H., Li L., and Huang C.: Chemical composition of PM2.5 and meterological impact among three years in urban Shanghai, China, Journal of Cleaner Proeuction, 112, 2, 1302-1311, 2016b.

Wang, H., Lu, K., Chen, X., Zhu, Q., Chen, Q., Guo, S., Jiang, M., Li, X., Shang, D., Tan, Z., Wu, Y., Wu, Z., Zou, Q., Zheng, Y., Zeng, L., Zhu, T., Hu, M., and Zhang, Y.: High N2O5 Concentrations Observed in Urban Beijing: Implications of a Large Nitrate Formation Pathway, Environmental Science & Technology Letters, 4, 416-420, 10.1021/acs.estlett.7b00341, 2017.

Wang, J., Ge, X., Chen, Y., Shen, Y., Zhang, Q., Sun, Y., Xu, J., Ge, S., Yu, H., and Chen, M.: Highly time-resolved urban aerosol characteristics during springtime in Yangtze River Delta, China: insights from soot particle aerosol mass spectrometry, Atmospheric Chemistry and Physics, 16, 9109-9127, 10.5194/acp-16-9109-2016, 2016c.

Wang, J., Zhao, B., Wang, S., Yang, F., Xing, J., Morawska, L., Ding, A., Kulmala, M., Kerminen, V.-M., Kujansuu, J., Wang, Z., Ding, D., Zhang, X., Wang, H., Tian, M., Petäjä, T., Jiang, J., Hao, J., Particulate matter pollution over China and the effects of control policies, Science of the Total Environment, 584, 426-447, 2017a.

Wang, T., Nie, W., Gao, J., Xue, L. K., Gao, X. M., Wang, X. F., Qiu, J., Poon, C. N., Meinardi, S., Blake, D., Wang, S. L., Ding, A. J., Chai, F. H., Zhang, Q. Z., and Wang, W. X.: Air quality during the 2008 Beijing Olympics: secondary pollutants and regional impact, Atmospheric Chemistry and Physics, 10, 7603-7615, 2010.

Wang, T., Tham, Y. J., Xue, L. K., Li, Q. Y., Zha, Q. Z., Wang, Z., Poon, S. C. N., Dube, W. P., Blake, D. R., Louie, P. K. K., Luk, C. W. Y., Tsui, W., and Brown, S. S.: Observations of nitryl chloride and modeling its source and effect on ozone in the planetary boundary layer of southern China, J Geophys Res-Atmos, 121, 2476-2489, 10.1002/2015JD024556, 2016d.

Wang, X., and Zhang, Y.: Particulate Nitrate Formation in a Highly Polluted Urban Area: A Case Study by Single-Particle Mass Spectrometry in Shanghai Environ. Sci. Technol, 43, 3061-3066, 2009.

Wang, X., Ding, X., Fu, X., He, Q., Wang, S., Bernard, F., Zhao, X., and Wu, D.: Aerosol scattering coefficients and major chemical compositions of fine particles observed at a rural site in the central Pearl River Delta, South China, Journal of Environmental Sciences, 24, 72-77, 10.1016/s1001-0742(11)60730-4, 2012.

Wang, X. F., Chen, J. M., Sun, J. F., Li, W. J., Yang, L. X., Wen, L., Wang, W. X., Wang, X. M., Collett, J. L., Shi, Y., Zhang, Q. Z., Hu, J. T., Yao, L., Zhu, Y. H., Sui, X., Sun, X. M., and Mellouki, A.: Severe haze episodes and seriously polluted fog water in Ji'nan, China, Sci Total Environ, 493, 133-137, 2014.

Wang, X., Wang, H., Xue, L., Wang, T., Wang, L., Gu, R., Wang, W., Tham, Y. J., Wang, Z., Yang, L., Chen, J., and Wang, W.: Observations of N 2 O 5 and ClNO 2 at a polluted urban surface site in North China: High N 2 O 5 uptake coefficients and low ClNO 2 product yields, Atmospheric Environment, 156, 125-134, 10.1016/j.atmosenv.2017.02.035, 2017b.

Wen, L., Chen, J., Yang, L., Wang, X., Caihong, X., Sui, X., Yao, L., Zhu, Y., Zhang, J., Zhu, T., and Wang, W.: Enhanced formation of fine particulate nitrate at a rural site on the North China Plain in summer: The important roles of ammonia and ozone, Atmospheric Environment, 101, 294-302, 10.1016/j.atmosenv.2014.11.037, 2015.

Wen, L., Xue, L., Wang, X., Xu, C., Chen, T., Yang, L., Wang, T., Zhang, Q., and Wang, W.: Summertime fine particulate nitrate pollution in the North China Plain: increasing trends, formation mechanisms and implications for control policy, Atmospheric Chemistry and Physics, 18, 11261-11275, 10.5194/acp-18-11261-2018, 2018.

Xie, Y., Ding, A., and Nie, W.: Enhanced sulfate formation by nitrogen dioxide: Implications from in situ observations at the SORPES station Journal Of Geophysical Research: Atmospheres, 120, 12,679-612,964, 10.1002/, 2015.

Xue., J., and Yuan., Z.: Insights into factors afferting nitrate in PM2.5 in a polluted high NOx environment through hourly observations and size distribution measurements Journal of Geophysical Research: Atmospheres, 119, 4888-4902, 10.1002/, 2013.

Yang, T., Sun, Y., Zhang, W., Wang, Z., Liu, X., Fu, P., and Wang, X.: Evolutionary processes and sources of high-nitrate haze episodes over Beijing, Spring, J Environ Sci (China), 54, 142-151, 10.1016/j.jes.2016.04.024, 2017.

Young, D. E., Kim, H., Parworth, C., Zhou, S., Zhang, X., Cappa, C. D., Seco, R., Kim, S., and Zhang, Q.: Influences of emission sources and meteorology on aerosol chemistry in a polluted urban environment: results from DISCOVER-AQ California, Atmospheric Chemistry and Physics, 16, 5427-5451, 10.5194/acp-16-5427-2016, 2016.

Zhang, Q., Canagaratna, M. R., Jayne, J. T., Worsnop, D. R., and Jimenez, J. L.: Time- and size-resolved chemical composition of submicron particles in Pittsburgh: Implications for aerosol sources and

processes, J Geophys Res-Atmos, 110, 2005.

Zhang, Y., Tang, L., Yu, H., Wang, Z., Sun, Y., Qin, W., Chen, W., Chen, C., Ding, A., Wu, J., Ge, S., Chen, C., and Zhou, H.-c.: Chemical composition, sources and evolution processes of aerosol at an urban site in Yangtze River Delta, China during wintertime, Atmospheric Environment, 123, 339-349, 10.1016/j.atmosenv.2015.08.017, 2015a.

Zhang, Y. J., Tang, L. L., Wang, Z., Yu, H. X., Sun, Y. L., Liu, D., Qin, W., Canonaco, F., Prévôt, A. S. H., Zhang, H. L., and Zhou, H. C.: Insights into characteristics, sources, and evolution of submicron aerosols during harvest seasons in the Yangtze River delta region, China, Atmospheric Chemistry and Physics, 15, 1331-1349, 10.5194/acp-15-1331-2015, 2015b.

Zhang, Y. W., Zhang, X. Y., Zhang, Y. M., Shen, X. J., Sun, J. Y., Ma, Q. L., Yu, X. M., Zhu, J. L., Zhang, L., and Che, H. C.: Significant concentration changes of chemical components of PM1 in the Yangtze River Delta area of China and the implications for the formation mechanism of heavy haze-fog pollution, The Science of the total environment, 538, 7-15, 10.1016/j.scitotenv.2015.06.104, 2015c.

Zhang, Y., Ding, A., Mao, H., Nie, W., Zhou, D., Liu, L., Huang, X., and Fu, C.: Impact of synoptic weather patterns and inter-decadal climate variability on air quality in the North China Plain during 1980-2013, Atmos. Environ., 124, 119-128, 2016.

Zou, J., Liu, Z., Hu, B., Huang, X., Wen, T., Ji, D., Liu, J., Yang, Y., Yao, Q., and Wang, Y.: Aerosol chemical compositions in the North China Plain and the impact on the visibility in Beijing and Tianjin, Atmospheric Research, 201, 235-246, 10.1016/j.atmosres.2017.09.014, 2018.

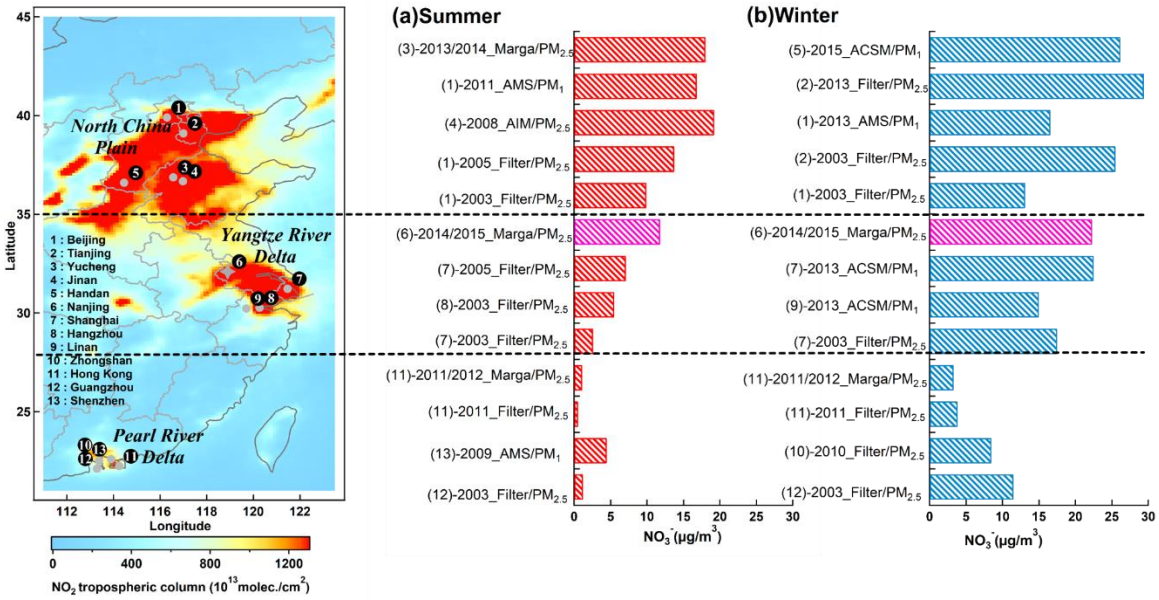

Figure 1 Average mass concentrations of particulate nitrate at different sampling sites in **(a)** summer and **(b)** winter. The left panel shows the map color-coded by 2-years (2014-2015) averaged tropospheric NO_2 from OMI satellite (http://www.temis.nl/airpollution/no2.html). The pink bars are for this study.

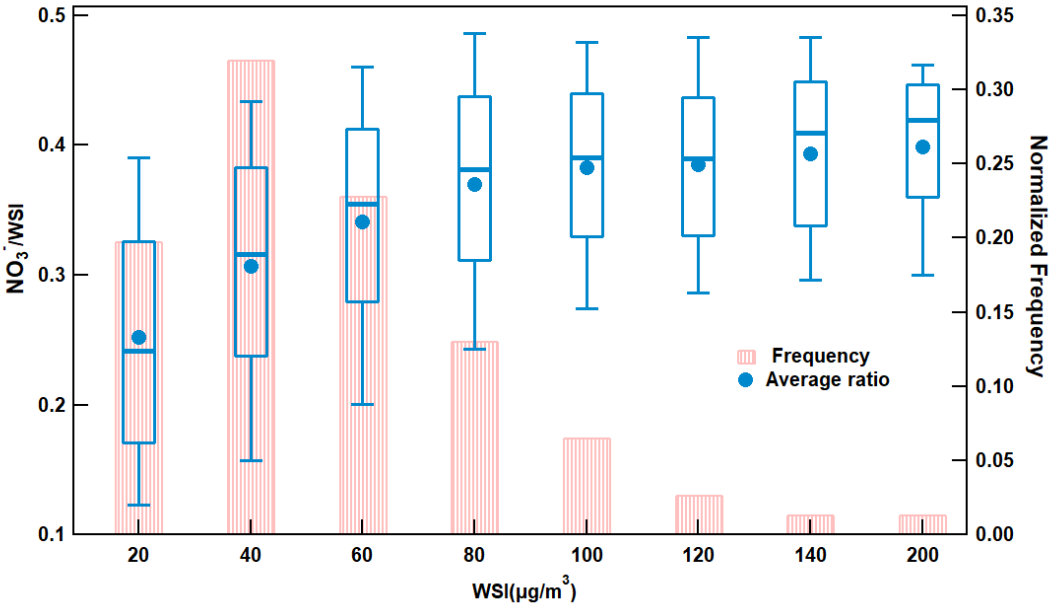

Figure 2 Average proportion of nitrate and normalized frequency of occurrence at different mass concentration bins of water soluble ions at SORPES. For the ratio, box boundaries represent the interquartile range, bars represent 5%-95% percentile range, and horizontal lines represent the median value.

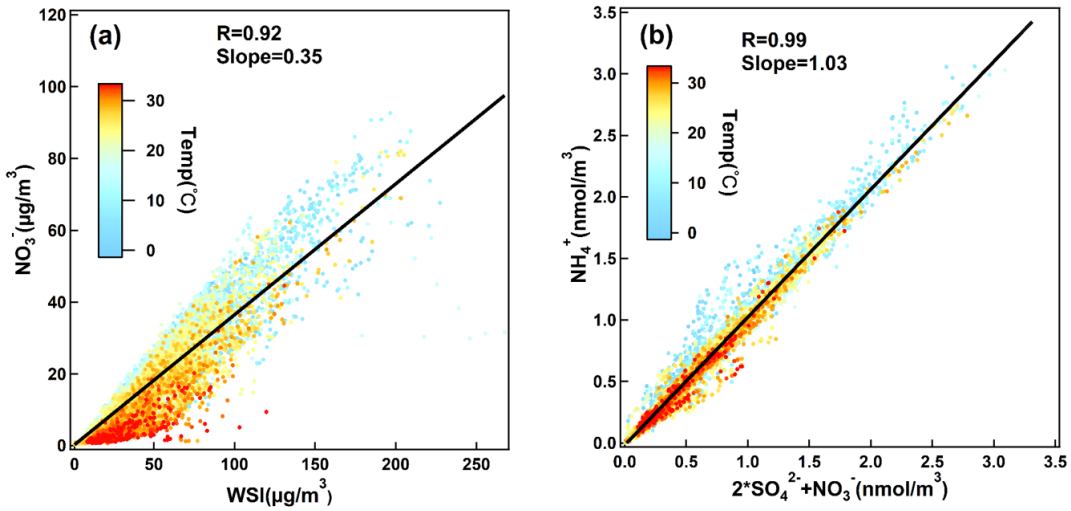

Figure 3 Scatter plots of **(a)** nitrate vs. total WSI color coded by air temperature, **(b)** molar concentrations of ammonium with nitrate molar concentrations plus two times of sulfate molar concentrations.

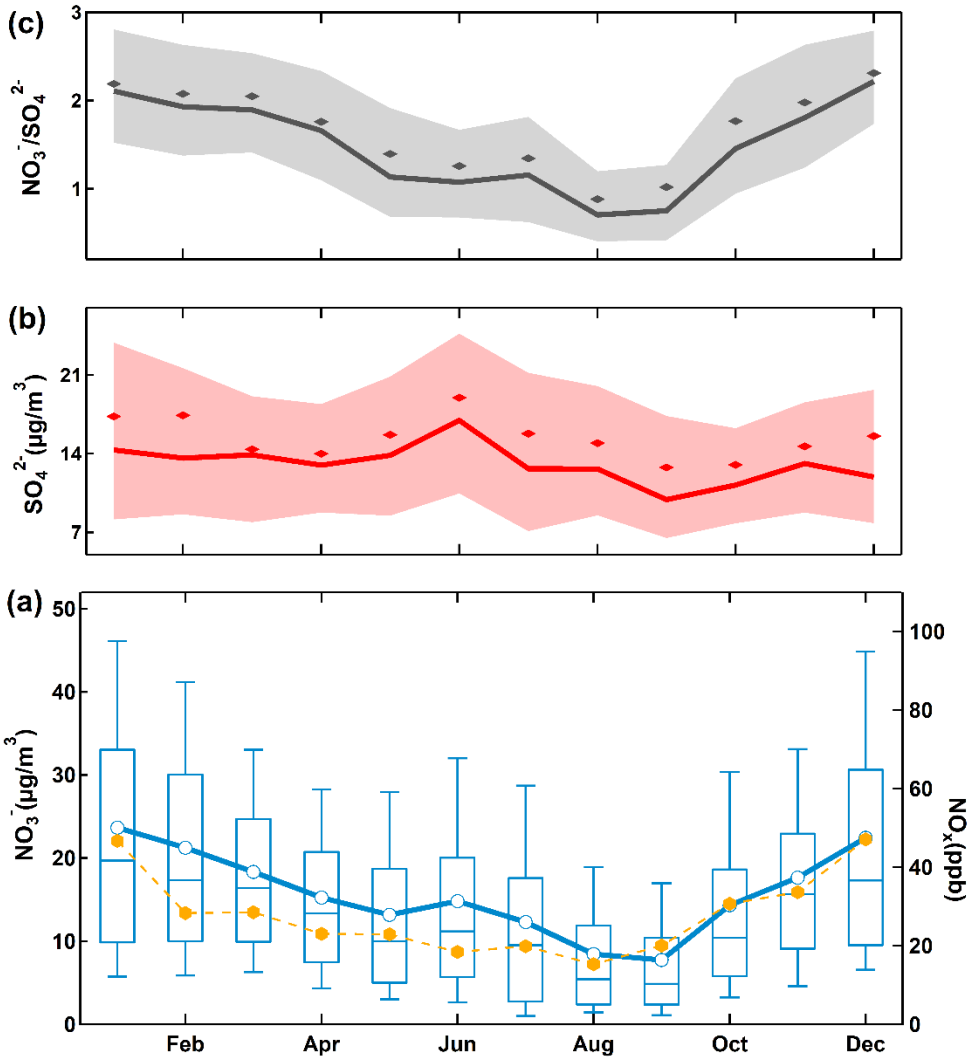

Figure 4 Monthly averaged nitrate (blue), sulfate (red), NO_x (orange) mass concentrations and nitrate to sulfate molar-based ratio (grey) measured at SORPES station during March 2014 to February 2016. For nitrate to sulfate ratio (a) and sulfate (b), bold solid lines are the median values, shade areas represent percentiles of 75% and 25%, and diamonds represent the mean values. For nitrate (c), box boundaries represent the interquartile range, bars represent 5%-95% percentile range, horizontal lines represent the median value, and crosses represent mean values.

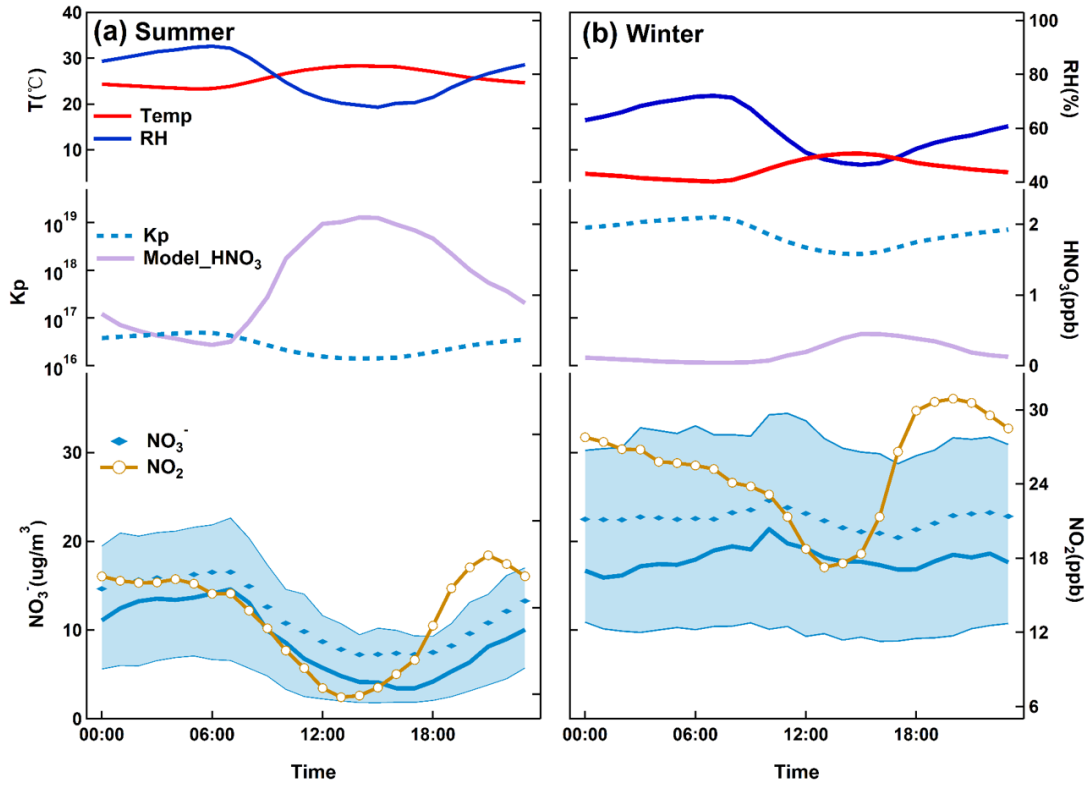

Figure 5 Diurnal variation of particulate nitrate in **(a)** summer and **(b)** winter. For nitrate, bold solid lines are the median values, shaded areas represent percentiles of 75% and 25% and diamonds represent mean values. Diurnal averages of NO_2 and modeled nitric acid mass concentrations are also provided with temperature and RH.

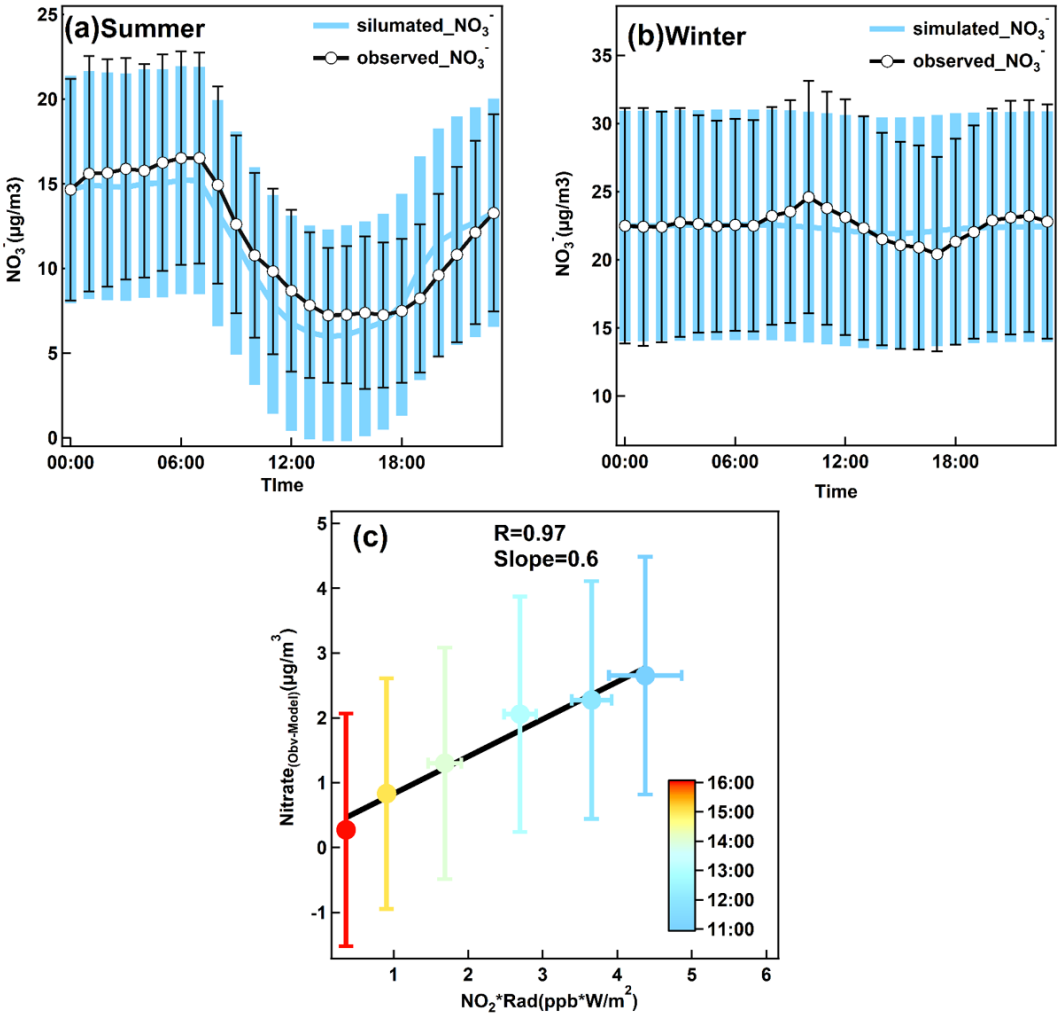

Figure 6 Modeled nitrate diurnal variations in **(a)** summer and **(b)** winter, together with the observed nitrate concentrations. Error bars provided are the standard deviation of the mean at each hourly interval. **(c)** Scatter plot of the difference between model and observed nitrate average mass concentrations with the product of NO_2 and radiation color coded by the hour of day for the samples.

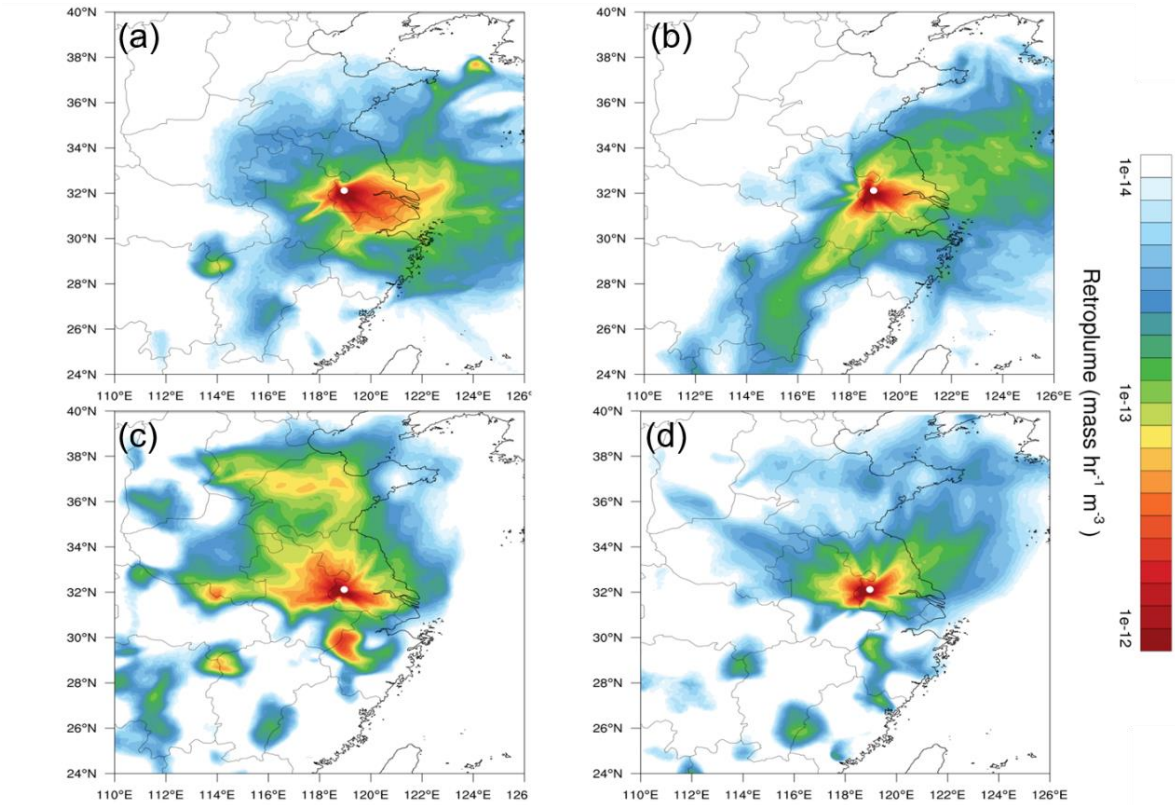

Figure 7 The averaged retroplumes (i.e., 100 m footprint) of the selected events: **(a)** Top 25% nitrate concentrations in summer, **(b)** Bottom 25% nitrate concentrations in summer, **(c)** Top 25% nitrate concentrations in winter, and **(d)** Bottom 25% nitrate concentrations in winter.

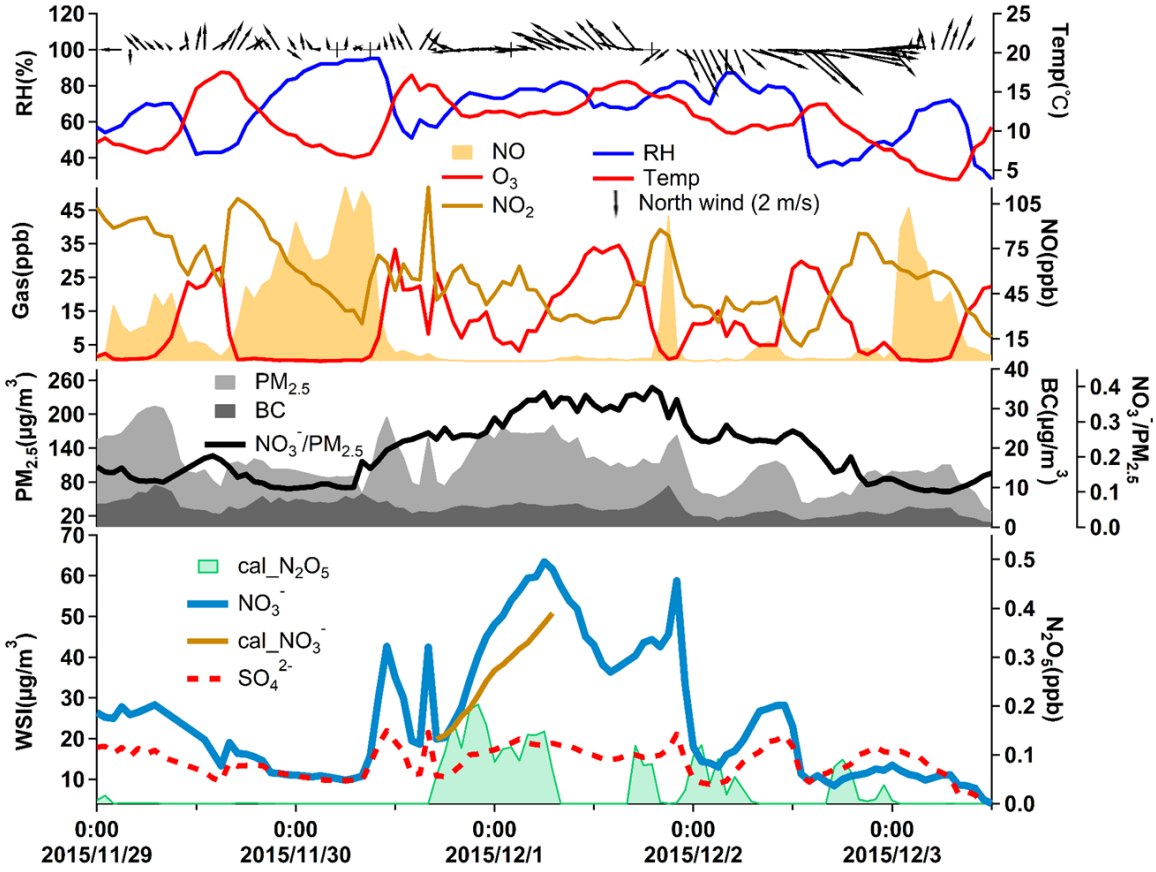

Figure 8 Time series of meteorological data and the concentrations of trace gases related to nitrate formation during 29 November to 3 December, 2015. Cal_NO_3^- represents the nitrate concentrations calculated from the hydrolysis of N_2O_5.

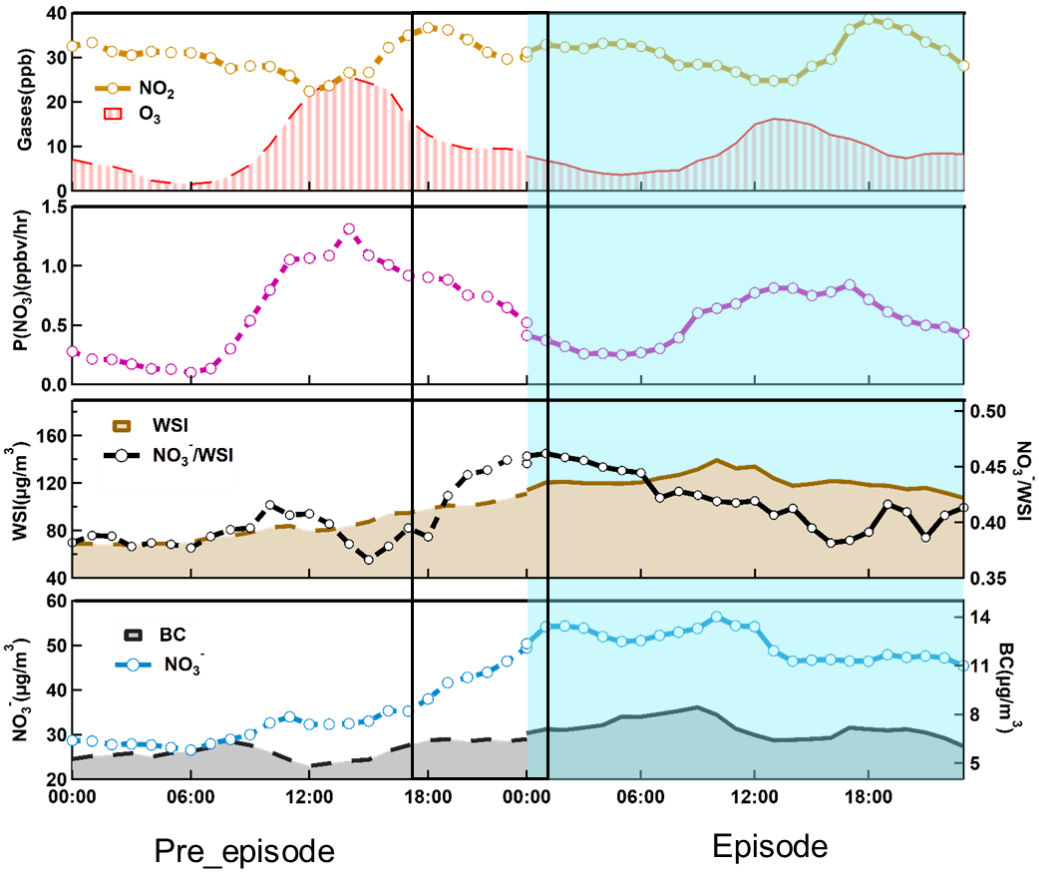

Figure 9 Diurnal variations of particulate nitrate, black carbon, the total water soluble ions, nitrate to WSI ratio, P (NO_3), NO_2, and O_3 averaged for nitrate episode days with exceedances of one mean plus two standard deviations. The left side shows the pre-episode days and the right side shows the episode days during the winter of entire two years period. The solid line box corresponds to the rapid growth of nitrate at night. It should be noted that P(NO_3) is calculated by the product of NO_2 and O_3 multiplied by the rate constant k_1 of NO_2+O_3 reaction.

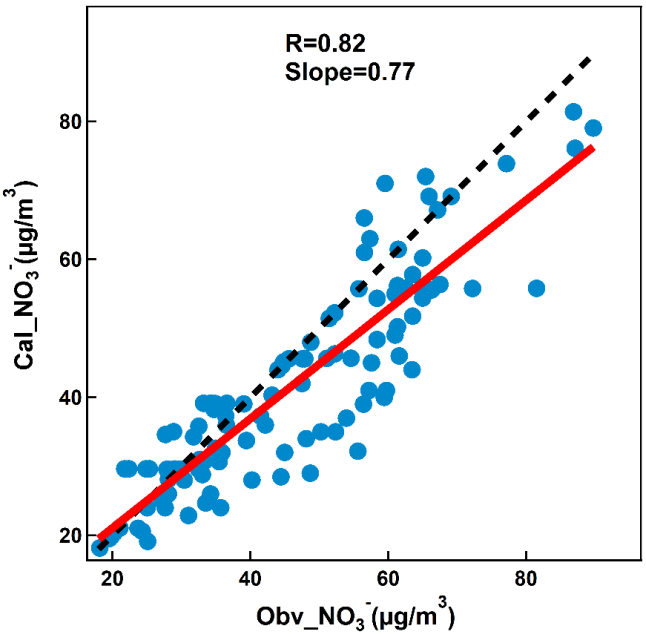

Figure 10 Scatter plot of calculated nitrate concentrations and observed nitrate concentrations from 17:00 to 23:00 of each episode.

Table 1 major gas phase and heterogeneous reactions involved NO_3 and N_2O_5

Reaction	Rate constant
$NO_2+O_3 \rightarrow NO_3+O_2$	$k_1=1.28\times10^{13}\times EXP(-2470/T)$
$NO_3+NO_2 \leftrightarrow N_2O_5$	$k_{eq}=1.73\times10^{-13}\times EXP(1550/T)$
$NO_3+NO \leftrightarrow NO_2+NO_2$	$k_3=1.8\times10^{-11}\times EXP(110/T)$
$NO_3 \rightarrow NO+O_2$	j_4
$NO_3 \rightarrow NO+O_2$	j_5
$NO_3 \xrightarrow{voc}$ products	$k_6=\sum(k_{voci}\cdot[voc]_i)$
$NO_3 \xrightarrow{Heterogeneous}$ products	$k_7=0.25\cdot i\cdot C_{NO_3}\cdot\gamma_{NO_3}\cdot S_{aerosol}$
$N_2O_5 \xrightarrow{Heterogeneous}$ products	$k_8=0.25\cdot C_{N_2O_5}\cdot\gamma_{N_2O_5}\cdot S_{aerosol}$